Ingale, V.V., Bazin, S., Olive, J.A., Briais, A. & Royer, J.Y., 2023. Hydroacoustic study of a seismic swarm in 2016–2017 near the Melville Transform Fault on the Southwest Indian Ridge, Bull. Seismol. Soc. Am., 113, 1523-1541, doi: 10.1785/0120220213.

Supplementary Material

Hydroacoustic study of a seismic swarm in 2016-2017 near the Melville Transform Fault on the Southwest Indian Ridge

Vaibhav Vijay Ingale, Sara Bazin, Jean-Arthur Olive, Anne Briais, and Jean-Yves Royer

Description

This file provides plots of waveforms and spectrograms of a few T-waves; of RLs for some representative events; of the improvements in the location and time errors; of the ISC catalog events along the SWIR from 2010 to 2020; of impulsive signal waveforms from this study and that of a dvolcano off Mayotte Island; of the spatio-temporal distribution as well as modified Omori's law fitting of the sequences studied; of the number of hydroacoustic events with respect to tidal heights.

List of Supplementary Figures

- **Figure S1:** Comparison of spectrograms and waveforms of some representative T-wave signals
- **Figure S2:** Corrections in source level (SL) of events based on received level (RL) for each hydrophone
- **Figure S3:** Improvements in error distribution after two picking iterations
- **Figure S4:** ISC catalog events along the SWIR axis
- **Figure S5:** Anomalous SL of events between January 09 and 20, 2017 and variations in RL for each hydrophone
- **Figure S6:** Spectrograms of S-SWIR and WKER2 hydrophones
- **Figure S7:** Comparison of impulsive events near the Melville TF and a volcano off Mayotte Island
- **Figure S8:** 09 June 2016 sequence #1
- **Figure S9:** 18 June 2016 sequence #2
- **Figure S10:** 30 June 2016 sequence #3
- **Figure S11:** 05 August 2016 sequence #4
- **Figure S12:** 25 August 2016 sequence #5
- **Figure S13:** 16 September 2016 sequence #6
- **Figure S14:** 02 October 2016 sequence #7
- **Figure S15:** 06 October 2016 sequence #8
- **Figure S16:** 26 December 2016 sequence #10
- **Figure S17:** 07 January 2017 sequence #11
- **Figure S18:** Distribution of earthquakes vs tidal heights

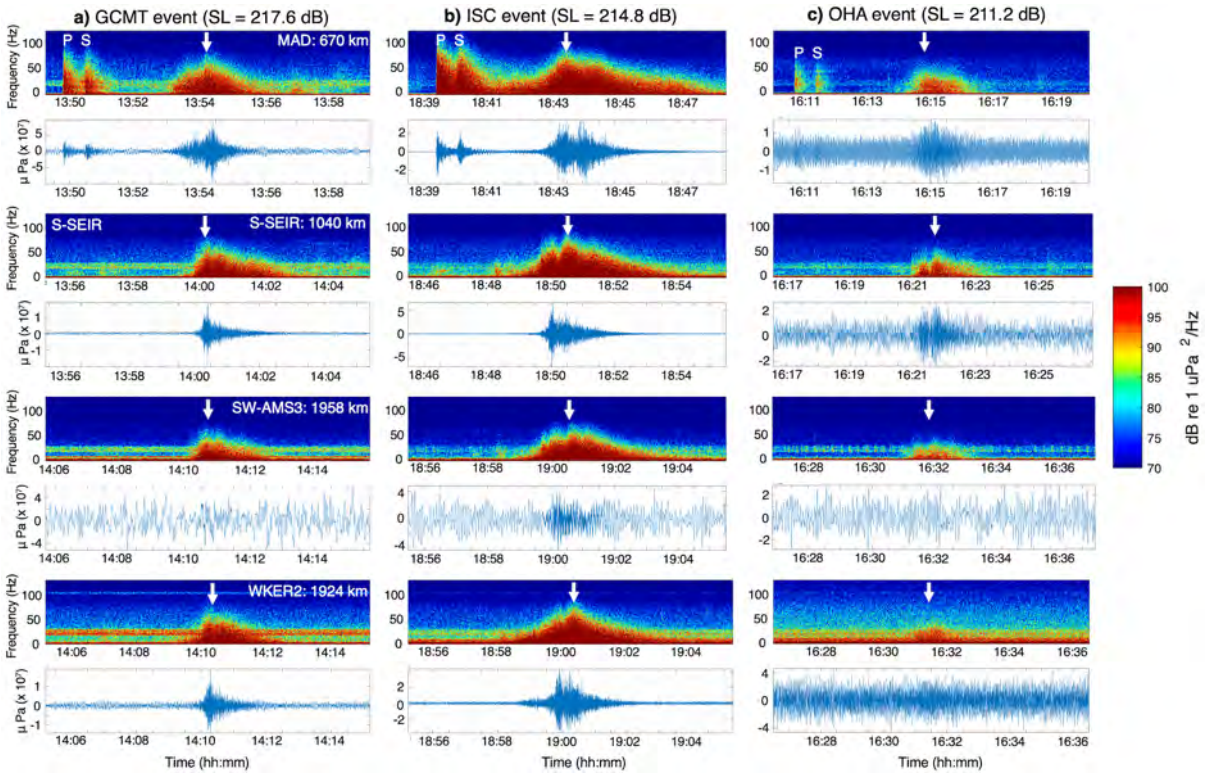

Figure S1 – Comparison of waveforms and spectrograms: Raw waveforms and spectrograms of some representative T-wave signals**: a)** ISC catalog event, **b)** GCMT catalog event; **c)** OHA catalog event, recorded at four hydrophones of the OHASISBIO network (MAD, S-SEIR, SW-AMS3, WKER2; from top to bottom); their distances in kilometers are from the reference point (cross in Figure 2). For all three events, the peak of T-wave energy (marked by arrows) occurs in the 0-60 Hz frequency range. Note that for the first two large events (*mb* = 4.7 and Mw = 5.5), the nearest hydrophone MAD (~ 670 km away) also recorded P and S wave arrivals, i.e., converted T-waves generated at the foot of the mooring.

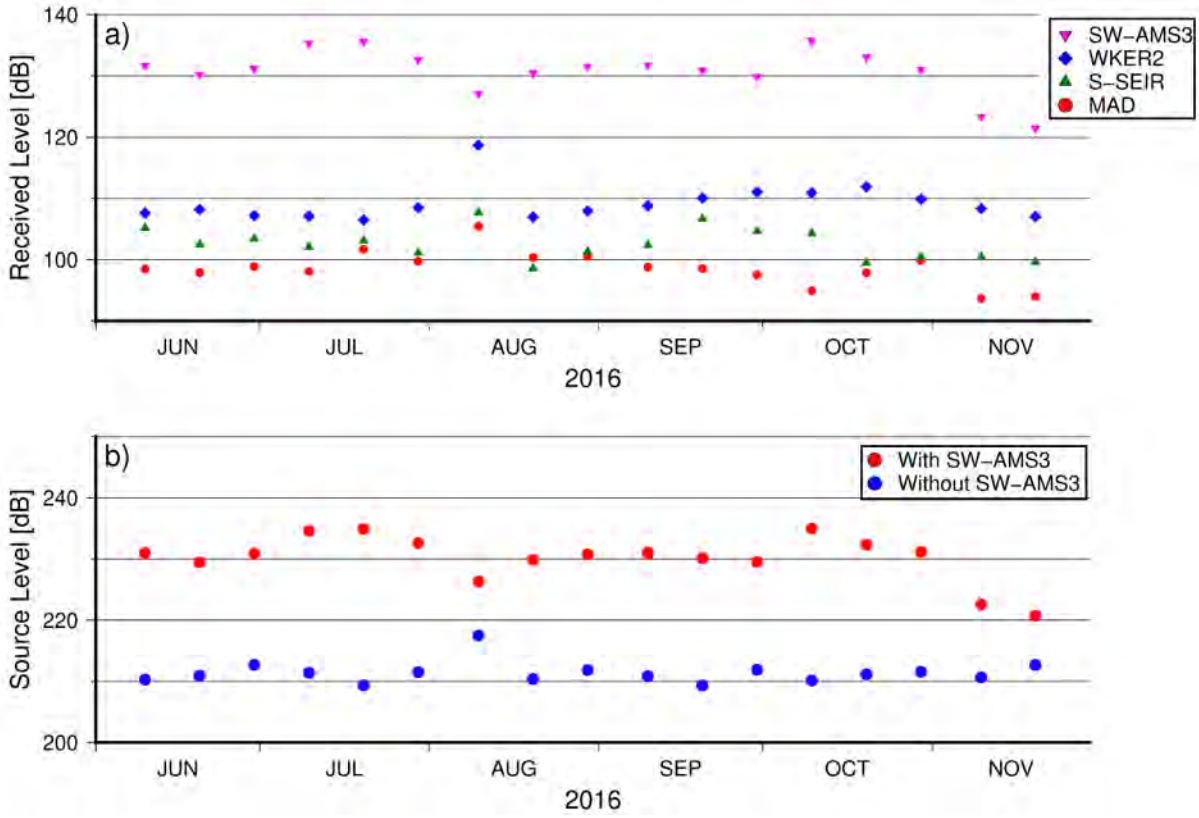

Figure S2 - Source Level corrections: a) Received Level (RL) in dB for a selection of events picked on SW-AMS3, WKER2, S-SEIR and MAD. Here SW-AMS3 has higher RL compared with the other three stations due to a higher sensor-sensitivity (see Table 1 in the paper). **b)** Source Level (SL) in dB for the events picked with (red) and without (blue) SW-AMS3. An averaged difference of 19.8 dB was applied to correct the SL of all events observed with SW-AMS3 in order to account for the network inhomogeneity in sensitivity.

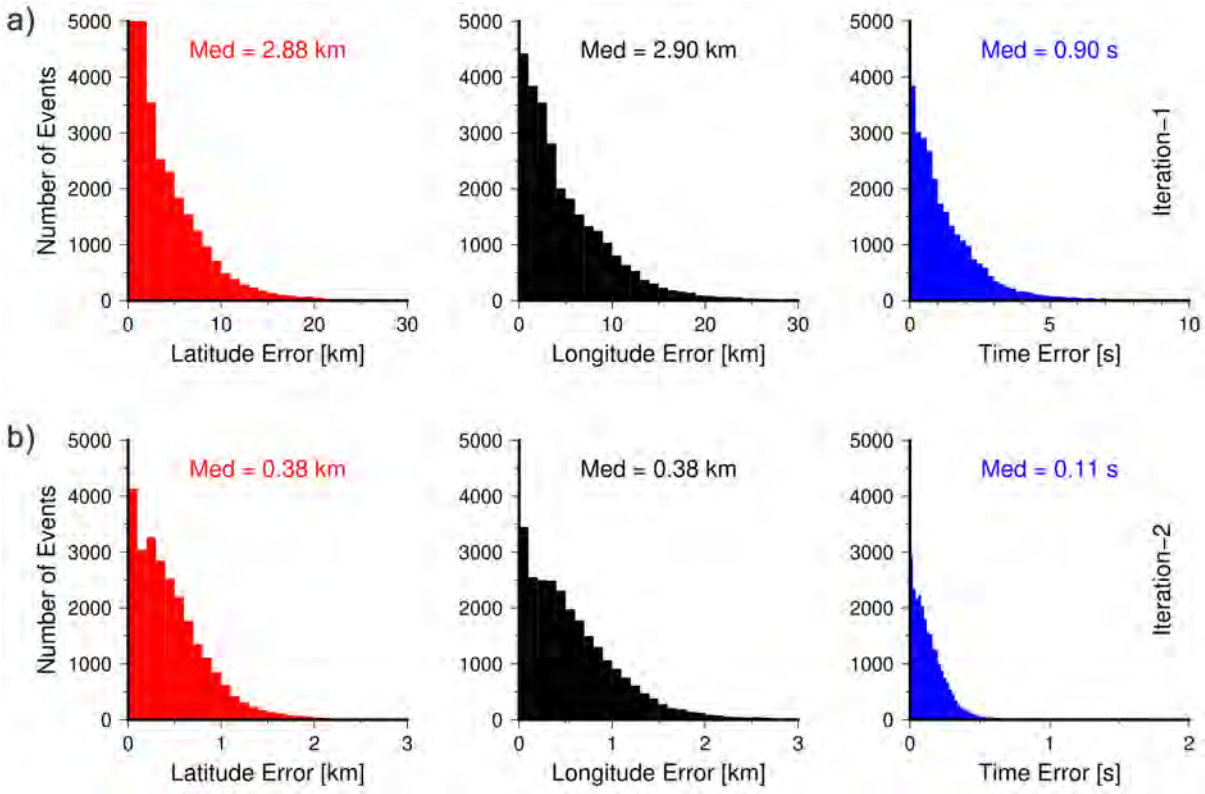

Figure S3 - Source localization errors: Errors obtained after acoustic triangulation in location (latitude and longitude) and origin time for all hydroacoustic events from the seismic cluster after the first (**top**) and second (**bottom**) picking iterations. Note here that x-axis scales are different in **a)** and **b)**.

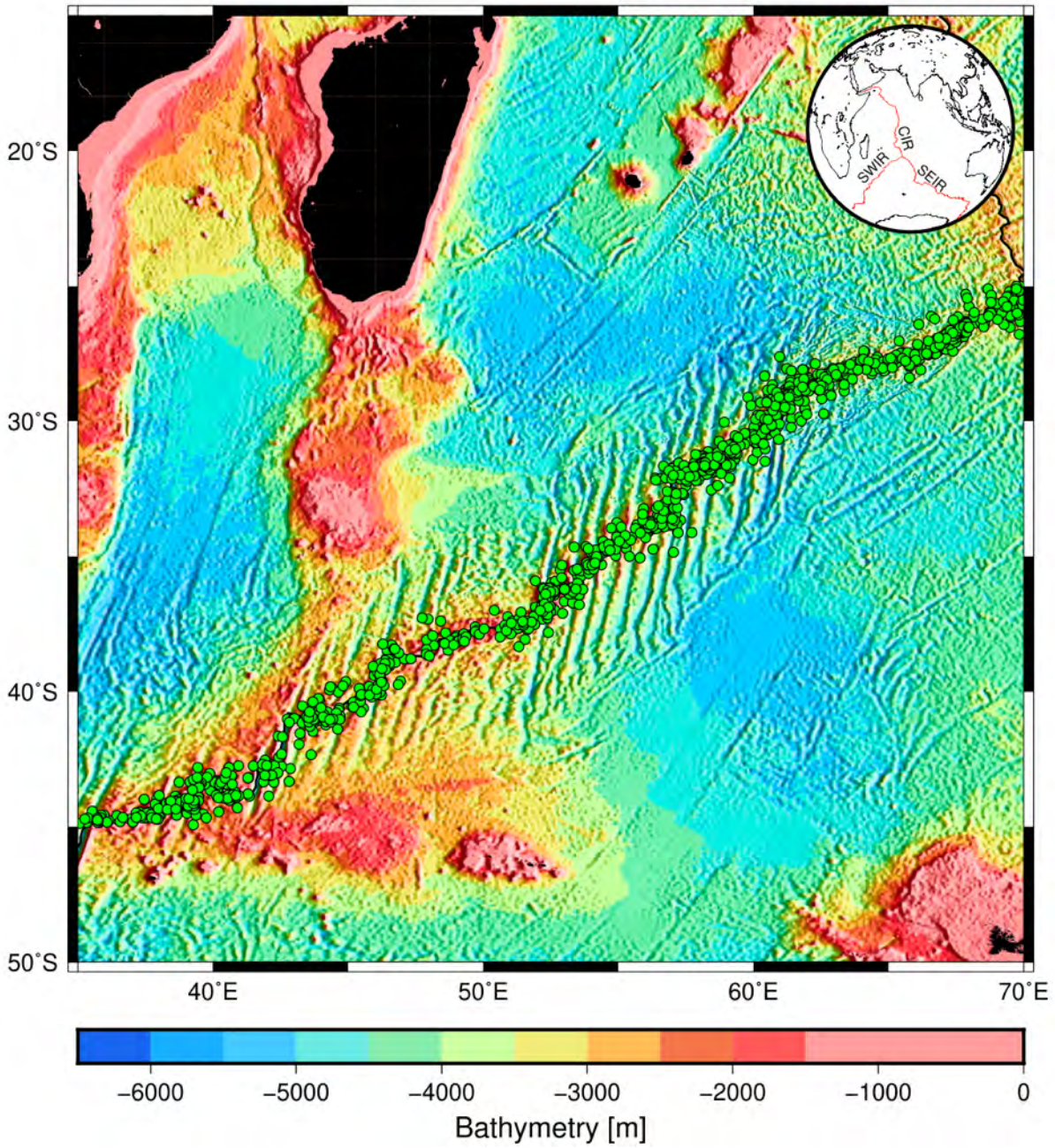

Figure S4 – ISC catalog of events along the SWIR axis: Geospatial distribution of 1933 events reported in the ISC catalog between 2010 and 2020 along the SWIR axis (ISC, 2022). Their magnitude (*mb*) is used for generating the trade-off between completeness of *mb* and SL of hydroacoustic events detected between June 2016 and March 2017 (Figure 3).

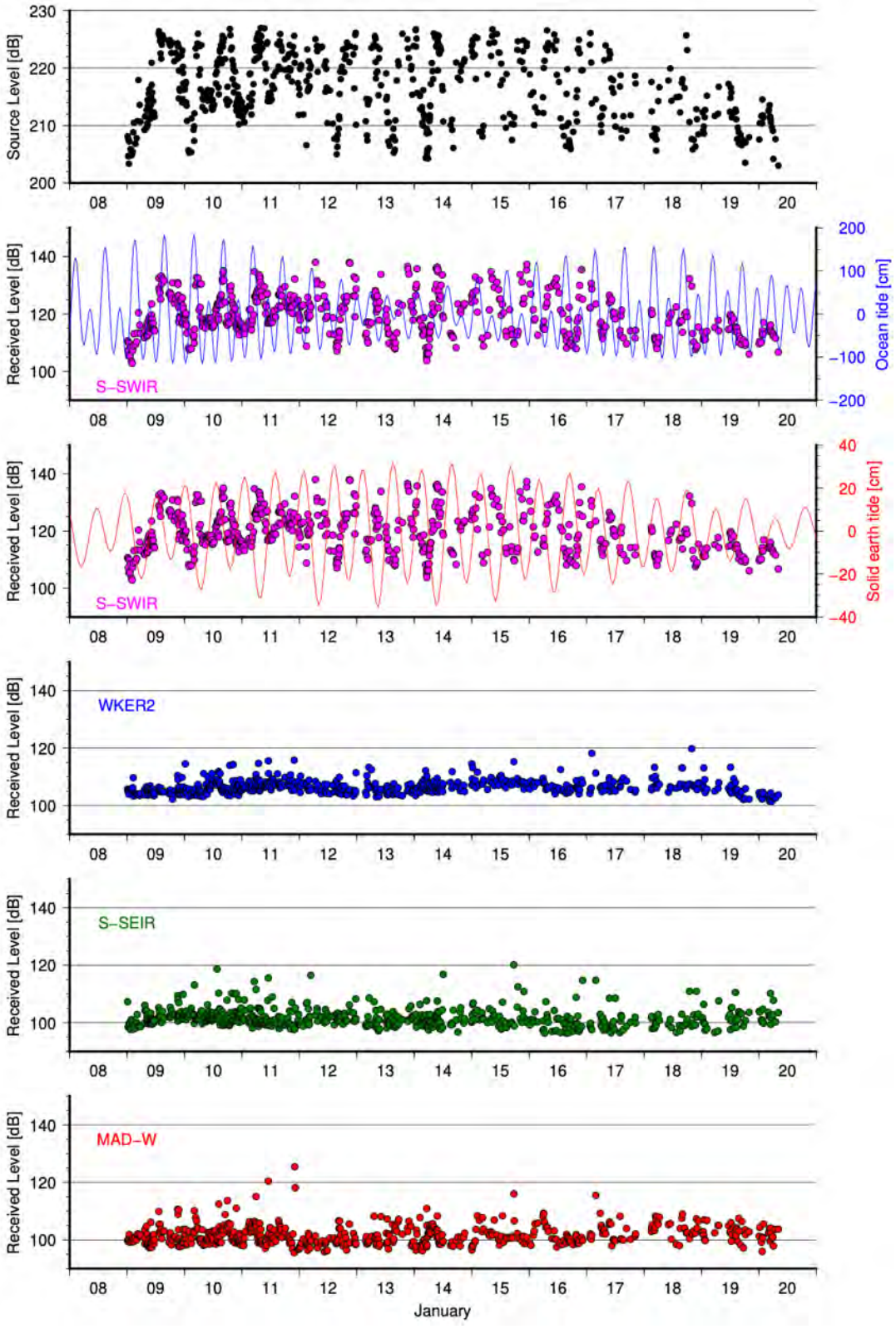

Figure S5 - Anomalous SL: Source Level of all events picked between January 8 and January 20, 2017 (black dots) compared to the received levels RL of these events at each hydrophone: S-SWIR (magenta dots), WKER2 (blue dots), S-SEIR (green dots), and MAD-W (red dots). Blue and red curves are ocean and solid Earth tidal heights, respectively.

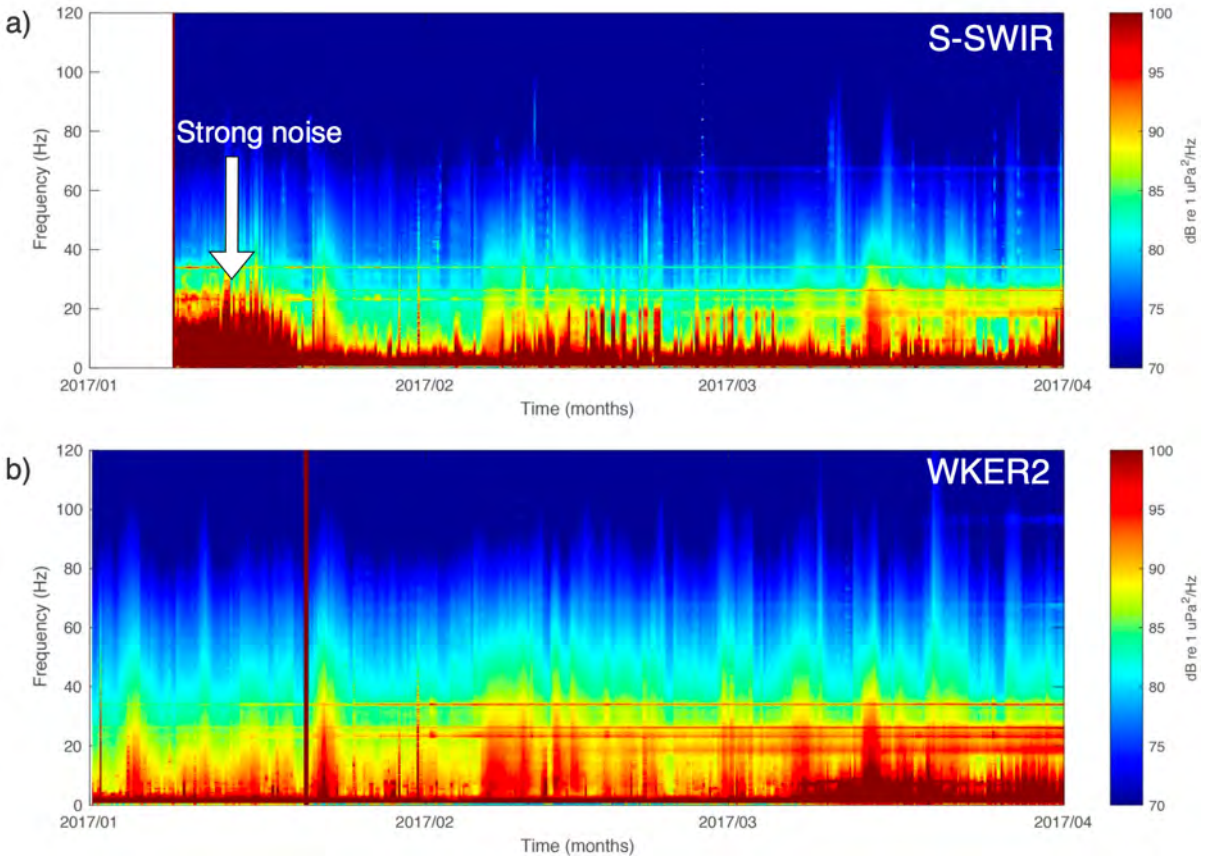

Figure S6 - Four-month long spectrograms at the S-SWIR and WKER2 sites in 2017 in the 0-120Hz frequency range (sampling rate is 240Hz). Each vertical line is a 6h-long average spectrum. The hydrophone sensitivities are -163.5 and -163.6 dB for S-SWIR and WKER2 respectively. A strong noise obscured the 0-30 Hz signal at the S-SWIR site in mid-January 2017.

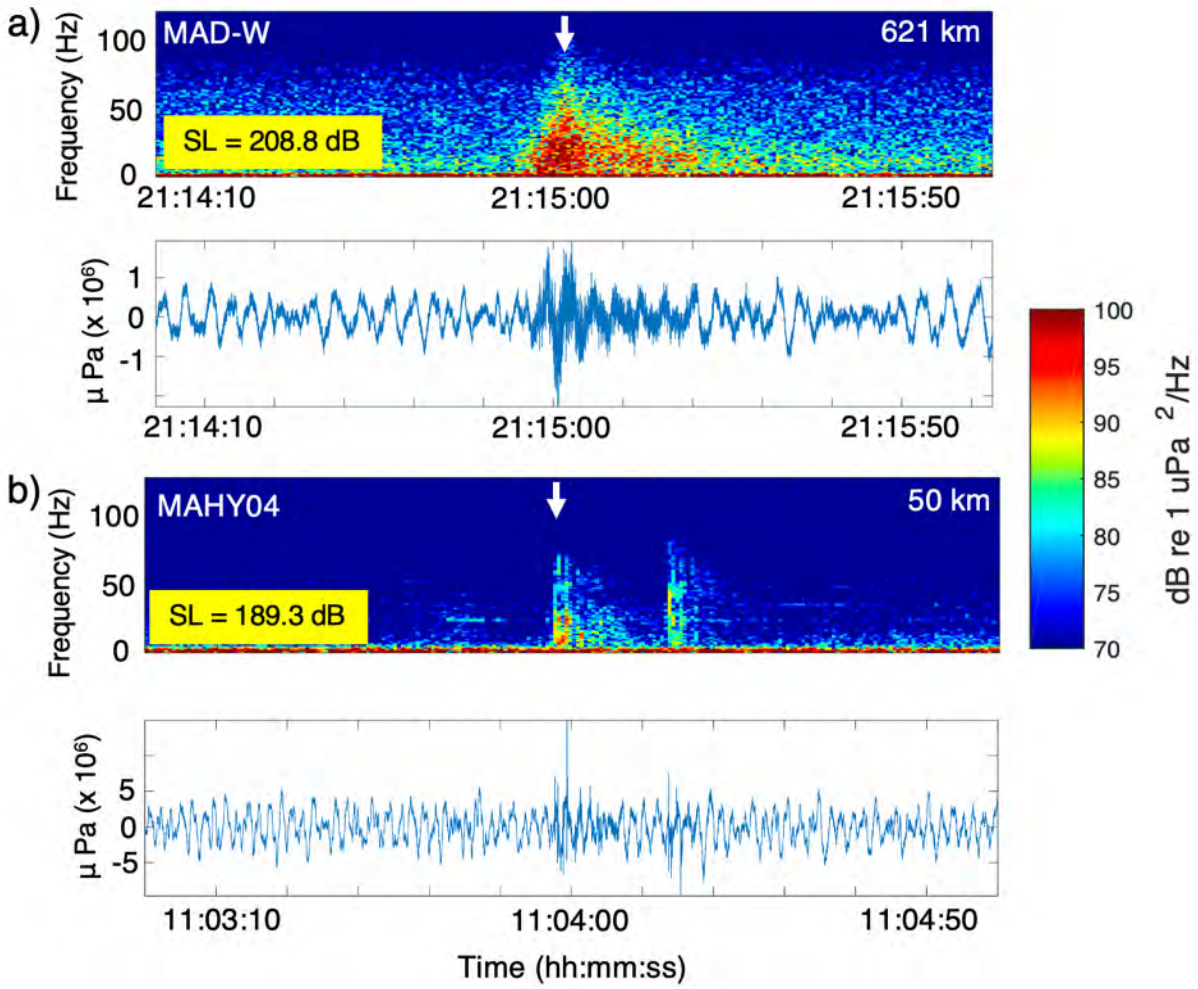

Figure S7 – Comparison of impulsive events near the Melville TF and near a volcano off Mayotte Island: Two-minute-long spectrograms and waveforms of an impulsive event recorded near the Melville TF (this study) and during a volcanic eruption off Mayotte Island (from Bazin et al., 2022). The event in **a)** is recorded 621 km away from the source (MAD-W), that in **b)** is recorded 50 km away (MAHY03) from the source. The SL is 208.8 dB for the first event vs. 189.3 dB for the second. Off Mayotte Island all impulsive events originate from recent active lava flows, mapped and observed from submersibles; the similarity in waveform and frequency contents of these two events suggests a common origin, that is interactions between hot lavas and seawater.

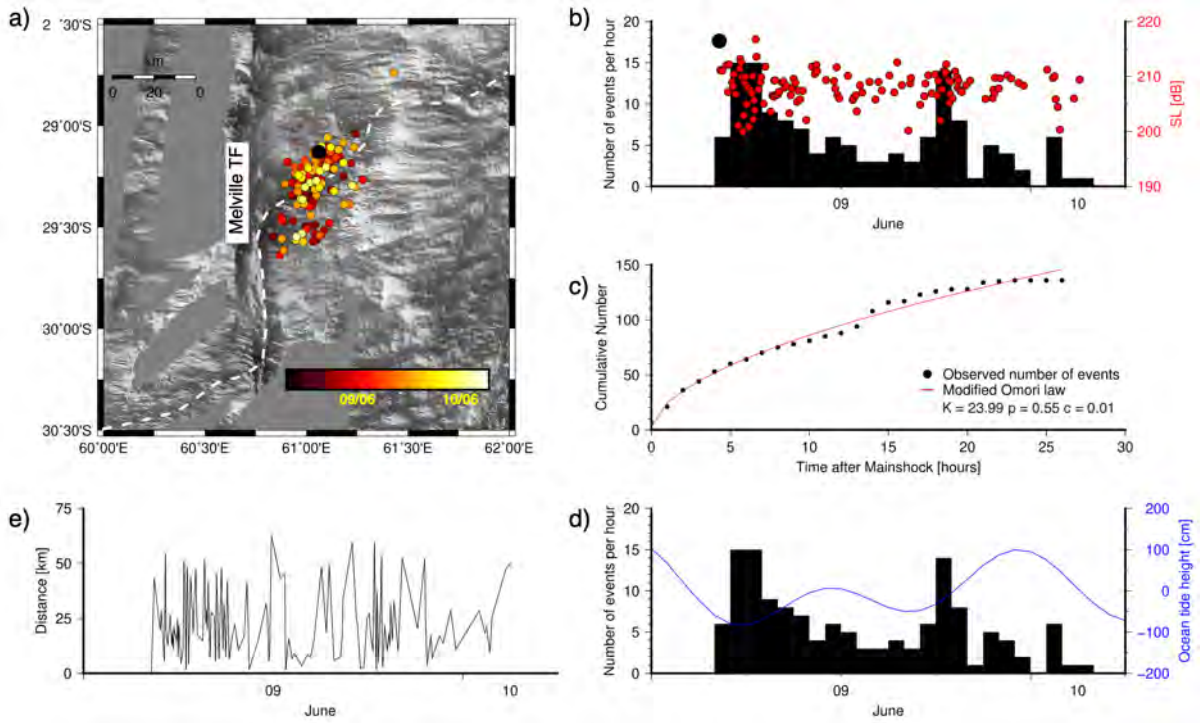

Figure S8 – 9th of June 2016 sequence 1: a) Spatio-temporal distribution of the events between June 09 and 10, 2016. The dashed line shows the SWIR axis. **b)** Histogram of number of events per hour in black color. Black and red circles show the SLs of T-waves for the first and following events, respectively. **c)** Black dots show the hourly cumulative number of events the red curve shows the modified Omori's law fit with the fitting parameters. **d)** Histogram of number of events per hour in black color and the ocean tide height in blue color. Tide height is computed with the Global Tidal Corrections program (Matsumoto et al., 2001). **e)** Distance of the events from the first event of the sequence.

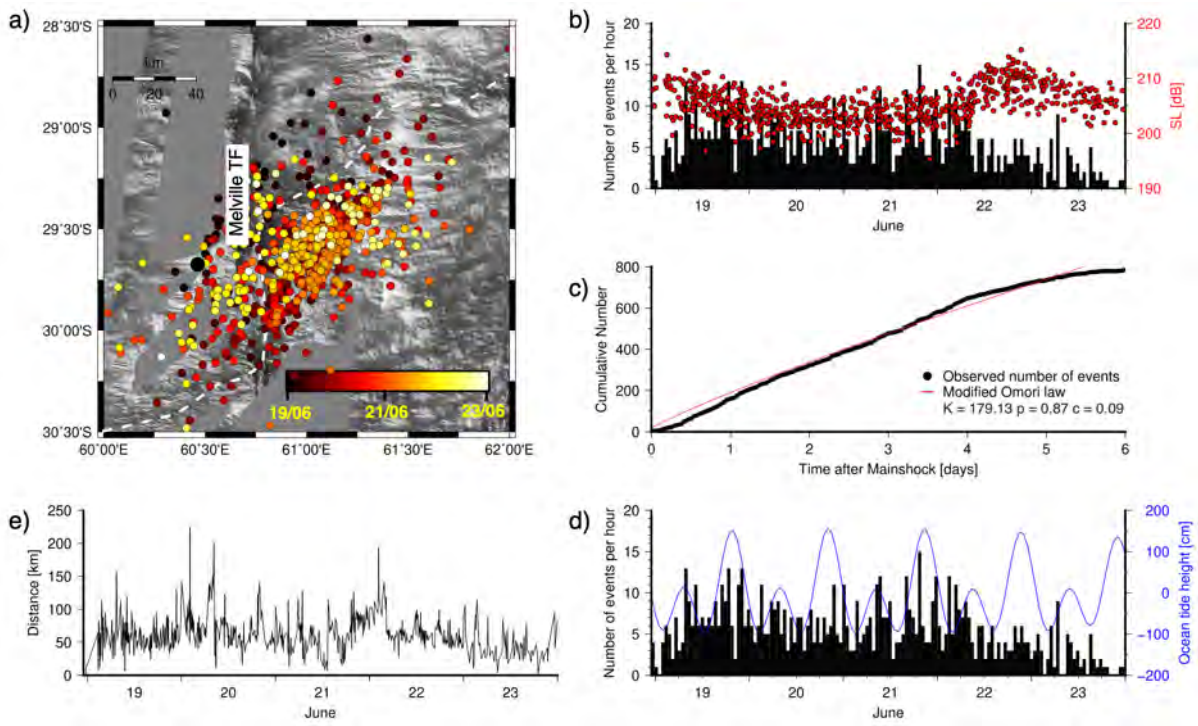

Figure S9 – 18th of June 2016 sequence 2: a) Spatio-temporal distribution of the events between June 18 and 23, 2016. The dashed line shows the SWIR axis. **b)** Histogram of number of events per hour in black color. Black and red circles show the SLs of T-waves for the first and following events, respectively. **c)** Black dots show the hourly cumulative number of events the red curve shows the modified Omori's law fit with the fitting parameters. **d)** Histogram of number of events per hour in black color and the ocean tide height in blue color. **e)** Distance of the events from the first event of the sequence.

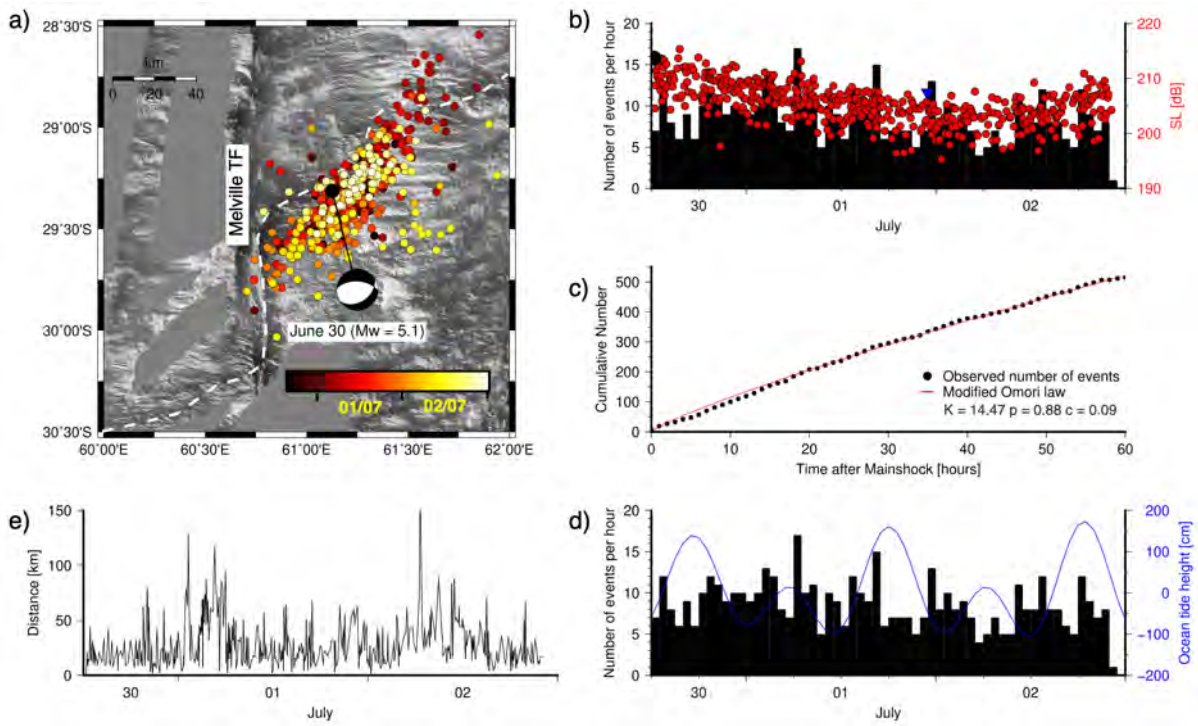

Figure S10 – 30th of June 2016 sequence 3: a) Spatio-temporal distribution of the events between June 30 and July 02, 2016. Beach ball show the normal faulting mechanism of GCMT event on June 30. The dashed line shows the SWIR axis. **b)** Histogram of number of events per hour in black color. Black and red circles show the SLs of T-waves for the first and following events, respectively. Blue triangles are SLs of impulsive events. **c)** Black dots show the hourly cumulative number of events the red curve shows the modified Omori's law fit with the fitting parameters. **d)** Histogram of number of events per hour in black color and the ocean tide height in blue color. **e)** Distance of the events from the first event of the sequence.

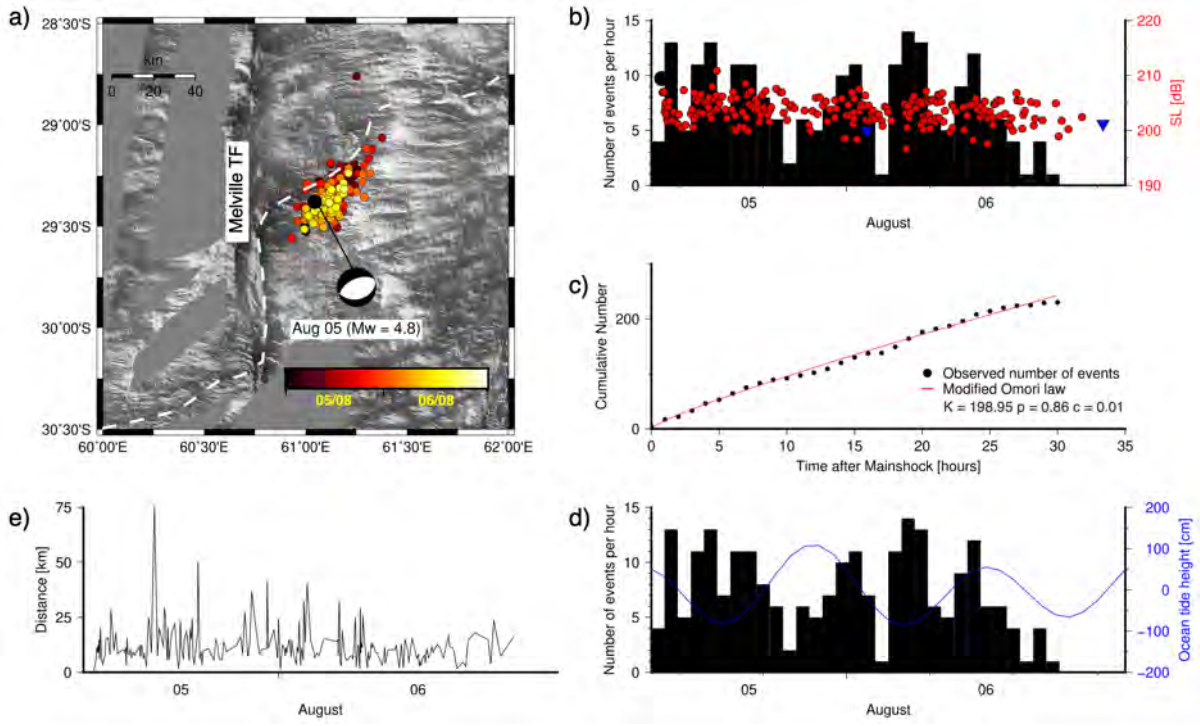

Figure S11 – 5th of August 2016 sequence 4: a) Spatio-temporal distribution of the events between August 05 and 06, 2016. Beach ball show the normal faulting mechanism of GCMT event on August 05. The dashed line shows the SWIR axis. **b)** Histogram of number of events per hour in black color. Black and red circles show the SLs of T-waves for the first and following events, respectively. Blue triangles are SLs of impulsive events. **c)** Black dots show the hourly cumulative number of events the red curve shows the modified Omori's law fit with the fitting parameters. **d)** Histogram of number of events per hour in black color and the ocean tide height in blue color. **e)** Distance of the events from the first event of the sequence.

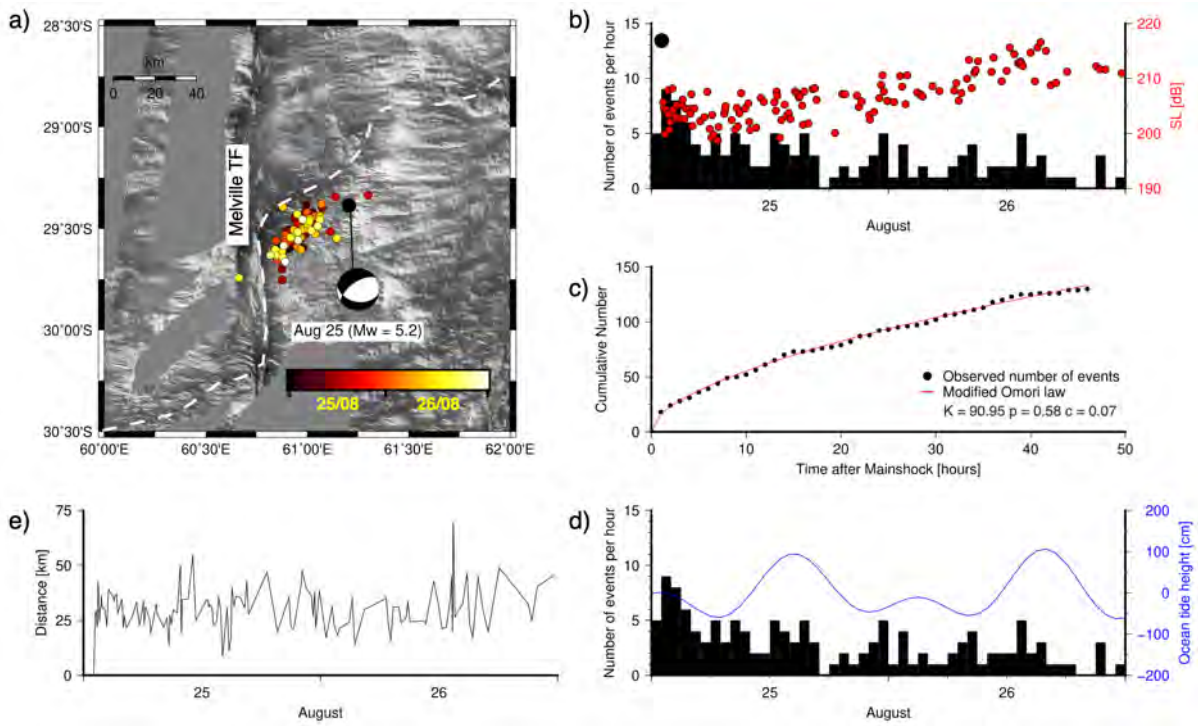

Figure S12 – 25th of August 2016 sequence 5: a) Spatio-temporal distribution of the events between August 25 and 26, 2016. Beach ball show the normal faulting mechanism of GCMT event on August 25. The dashed line shows the SWIR axis. **b)** Histogram of number of events per hour in black color. Black and red circles show the SLs of T-waves for the first and following events, respectively. **c)** Black dots show the hourly cumulative number of events the red curve shows the modified Omori's law fit with the fitting parameters. **d)** Histogram of number of events per hour in black color and the ocean tide height in blue color. **e)** Distance of the events from the first event of the sequence.

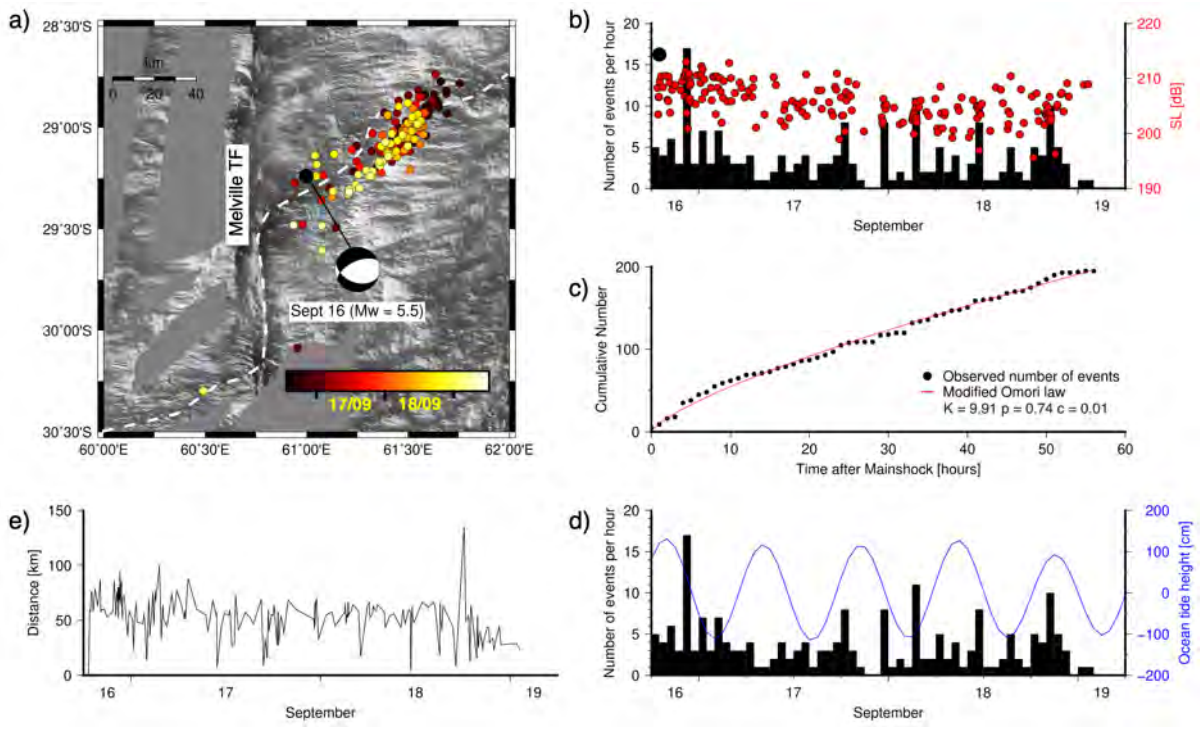

Figure S13 – 16th of September 2016 sequence 6: a) Spatio-temporal distribution of the events between September 16 and 19, 2016. Beach ball show the normal faulting mechanism of GCMT event on September 16. The dashed line shows the SWIR axis. **b)** Histogram of number of events per hour in black color. Black and red circles show the SLs of T-waves for the first and following events, respectively. **c)** Black dots show the hourly cumulative number of events the red curve shows the modified Omori's law fit with the fitting parameters. **d)** Histogram of number of events per hour in black color and the ocean tide height in blue color. **e)** Distance of the events from the first event of the sequence.

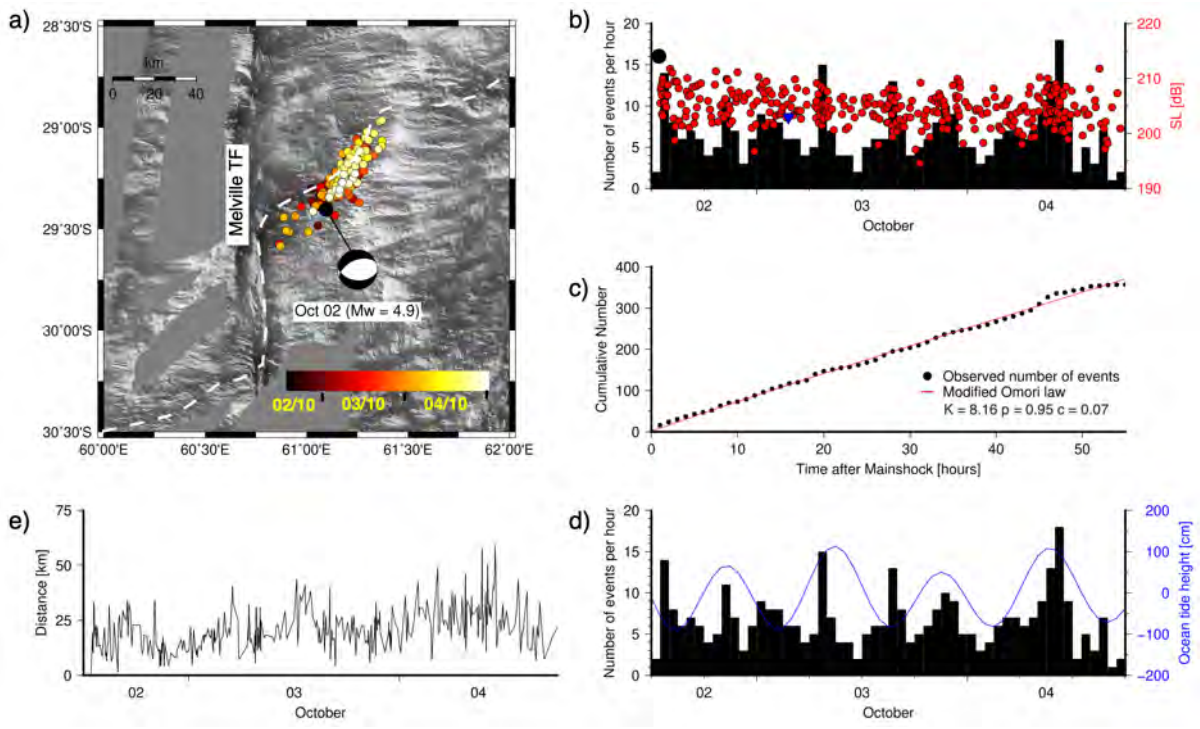

Figure S14 – 2nd of October 2016 sequence 7: a) Spatio-temporal distribution of the events between October 02 and 04, 2016. Beach ball show the normal faulting mechanism of GCMT event on October 02. The dashed line shows the SWIR axis. **b)** Histogram of number of events per hour in black color. Black and red circles show the SLs of T-waves for the first and following events, respectively. Blue triangles are SLs of impulsive events. **c)** Black dots show the hourly cumulative number of events the red curve shows the modified Omori's law fit with the fitting parameters. **d)** Histogram of number of events per hour in black color and the ocean tide height in blue color. **e)** Distance of the events from the first event of the sequence.

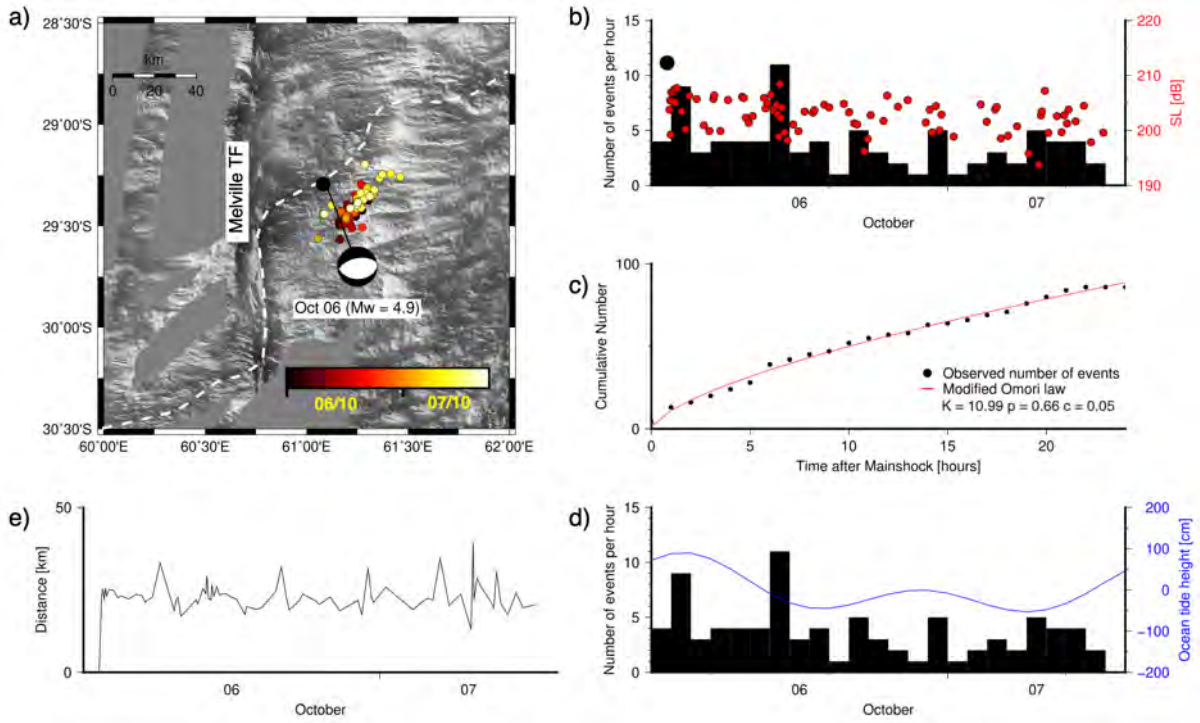

Figure S15 – 6th of October 2016 sequence 8: a) Spatio-temporal distribution of the events between October 06 and 07, 2016. Beach ball show the normal faulting mechanism of GCMT event on October 06. The dashed line shows the SWIR axis. **b)** Histogram of number of events per hour in black color. Black and red circles show the SLs of T-waves for the first and following events, respectively. **c)** Black dots show the hourly cumulative number of events the red curve shows the modified Omori's law fit with the fitting parameters. **d)** Histogram of number of events per hour in black color and the ocean tide height in blue color. **e)** Distance of the events from the first event of the sequence.

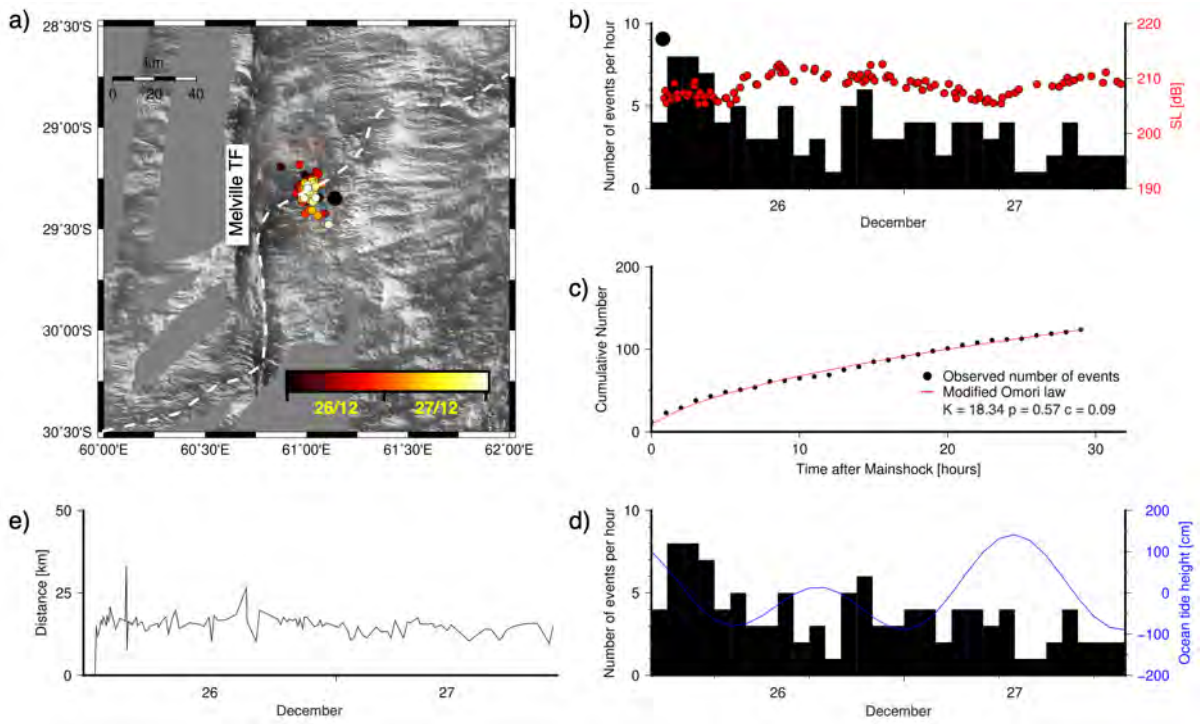

Figure S16 – 26th of December 2016 sequence 10: a) Spatio-temporal distribution of the events between December 26 and 27, 2016. The dashed line shows the SWIR axis. **b)** Histogram of number of events per hour in black color. Black and red circles show the SLs of T-waves for the first and following events, respectively. **c)** Black dots show the hourly cumulative number of events the red curve shows the modified Omori's law fit with the fitting parameters. **d)** Histogram of number of events per hour in black color and the ocean tide height in blue color. **e)** Distance of the events from the first event of the sequence.

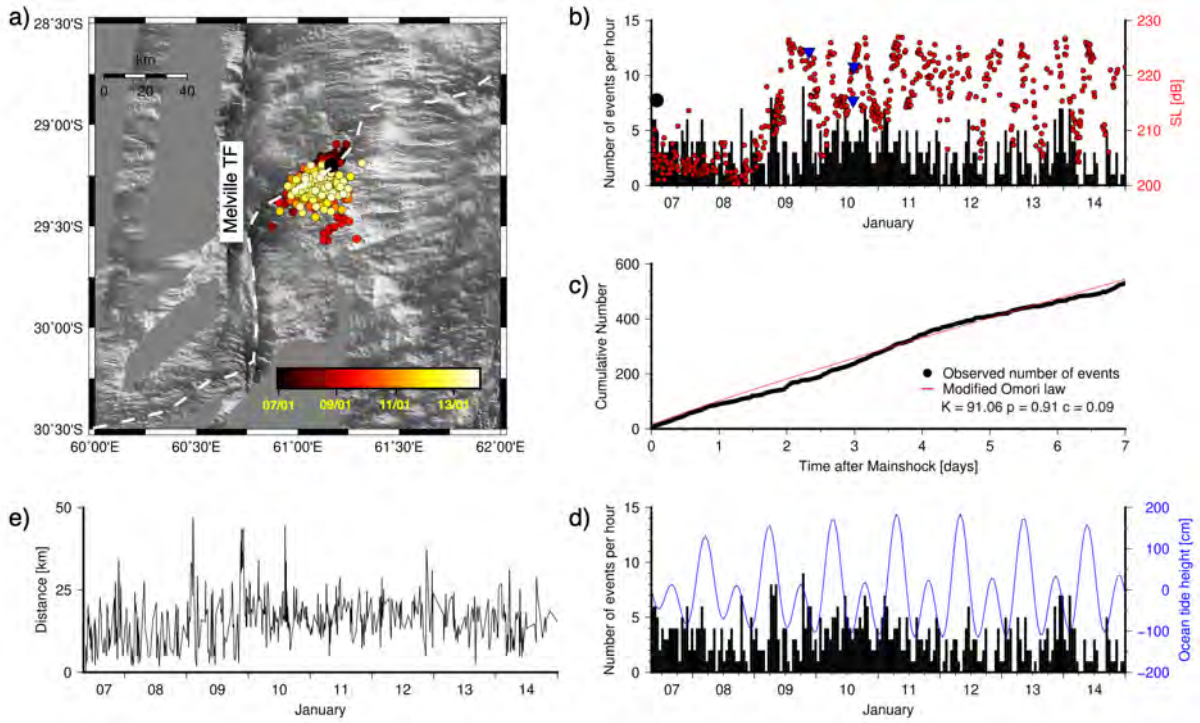

Figure S17 – 7th of January 2017 sequence 11: a) Spatio-temporal distribution of the events between January 07 and 14, 2017. The dashed line shows the SWIR axis. **b)** Histogram of number of events per hour in black color. Black and red circles show the SLs of T-waves for the first and following events, respectively. Blue triangles are SLs of impulsive events. **c)** Black dots show the hourly cumulative number of events the red curve shows the modified Omori's law fit with the fitting parameters. **d)** Histogram of number of events per hour in black color and the ocean tide height in blue color. **e)** Distance of the events from the first event of the sequence.

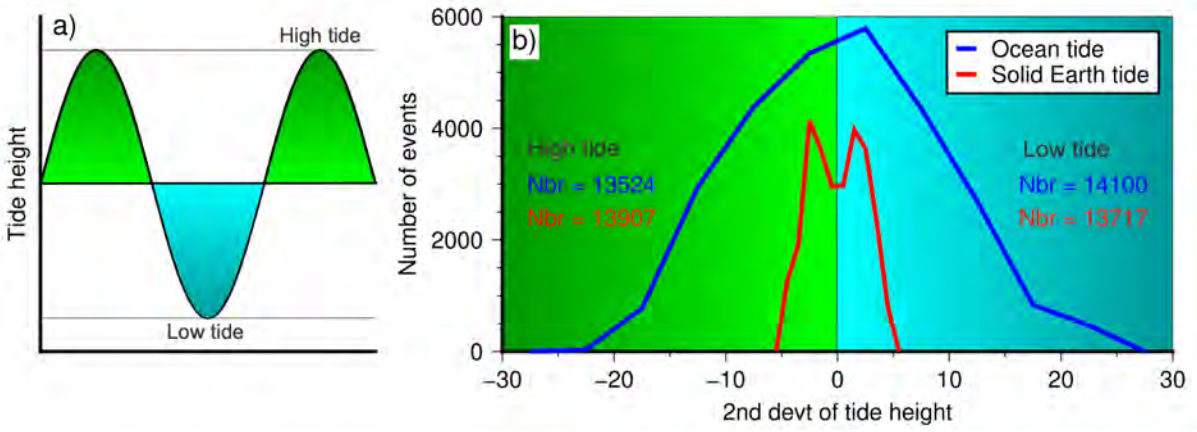

Figure S18 - Tidal effects on seismicity: a) Definitions of high tide (green) and low tide (cyan). **b)** Second derivative of ocean (blue curve) and solid-Earth tide (red curve). A positive 2nd derivative corresponds to low tide period (cyan colored region) and a negative 2nd derivative corresponds to high tide period (green colored region). Numbers represent the events counted during high tide (green side) and during low tide (cyan side); blue and red, fonts and curves, refer to the ocean or solid-Earth tides.

References

Bazin S., J.-Y., Royer, F. Dubost, F. Paquet, B. Loubrieu, A. Lavayssière, C. Deplus, N. Feuilet, É. Jacques, E. Rinnert, I. Thinon, E. Lebas, D. Pierre, L. Retailleau, J.-M. Saurel, A. Sukhovich, R. Bonnet and the REVOSIMA group (2022). Initial results from a hydroacoustic network to monitor submarine lava flows near Mayotte Island, *C. R. Geosci.* **1**, 0, doi: 10.5802/crgeos.119.

ISC International Seismological Center, On-Line Bulletin (2022). Available online: http://www.isc.ac.uk/iscbulletin/search/catalogue/ (last accessed on 10 January 2022).

Matsumoto, K., T. Sato, T. Takanezawa, and M. Ooe (2001). GOTIC2: A Program for Computation of Oceanic Tidal Loading Effect, *J. Geod. Soc. Jpm.* **47** (1), 243-248, doi: 10.11366/sokuchi1954.47.243.